

# Orbital Resonant Valence Bond States: Emergence of Superconductivity in Doped Multiorbital Chains

N. D. Patel,<sup>1</sup> N. Kaushal,<sup>2,3</sup> A. Nocera,<sup>2,4</sup> G. Alvarez,<sup>5</sup> and E. Dagotto<sup>2,3,\*</sup>

<sup>1</sup>*Department of Physics, The Ohio State University,  
191 W. Woodruff Avenue, Columbus, OH 43210*

<sup>2</sup>*Department of Physics and Astronomy, The University of Tennessee, Knoxville, Tennessee 37996, USA*

<sup>3</sup>*Materials Science and Technology Division, Oak Ridge National Laboratory, Oak Ridge, Tennessee 37831, USA*

<sup>4</sup>*Department of Physics and Astronomy and Stewart Blusson Quantum Matter Institute,  
University of British Columbia, Vancouver, B.C., Canada, V6T 1Z1*

<sup>5</sup>*Computer Science & Mathematics Division and Center for Nanophase Materials Sciences,  
Oak Ridge National Laboratory, Oak Ridge, Tennessee 37831, USA*

We introduce an ‘‘Orbital Resonant Valence Bond’’ (ORVB) state for two-orbital Hubbard models in one dimension that explains the recent computational discovery of pairing in these systems when hole doped. Our Ansatz is based on a mathematical expression where the undoped (one electron per orbital) quantum state of two nearest-neighbor (NN) sites coupled into a global spin singlet is rewritten exactly employing only spin-1/2 singlets linking NN orbitals. Generalizing to longer chains provides an ORVB variational state that can be visualized geometrically expressing our chain as a two-leg ladder, with one orbital per leg. As in Anderson’s resonating valence-bond state, ORVB describes the undoped ground state as a ‘‘liquid’’ of preformed NN singlet pairs that via doping become mobile. Real materials with one-dimensional substructures, two near-degenerate orbitals, and intermediate Hubbard  $U/W$  strengths –  $W$  the carrier’s bandwidth – could realize the ORVB state if on-site anisotropies are small. If these anisotropies are robust, spin-triplet pairing is possible.

**Introduction** — Quantum Materials merge topological concepts [1], such as in Haldane chains with non-local order parameters and edge states [2, 3], with electronic correlation effects, such as in iron-based superconductors with robust Hubbard  $U$  and Hund  $J_H$  couplings [4–7]. The Haldane chain started the field of topological materials and physical realization were reported in CsNiCl<sub>3</sub> [8], AgVP<sub>2</sub>S<sub>6</sub> [9], NENP [10], Y<sub>2</sub>BaNiO<sub>5</sub> [11], and PbNi<sub>2</sub>V<sub>2</sub>O<sub>8</sub> [12]. These chains have a spin gap as well as protected edge states when open boundary conditions (OBC) are used [3, 13–15]. In iron- and copper-based superconductors, most efforts employ planar geometries [16, 17] but Cu-oxide two-leg ladders were widely studied when they were predicted and confirmed to have a spin gap and become superconducting [18–22]. Recently, analogous developments occurred in iron materials when ladders BaFe<sub>2</sub>S<sub>3</sub> [23–25] and BaFe<sub>2</sub>Se<sub>3</sub> [26, 27] were reported to become superconducting with pressure. The study of iron ladders is vast and already revealed interesting complex magnetic states [23–42]. However, similar efforts using iron chains, such as in TlFeSe<sub>2</sub> or TlFeS<sub>2</sub>, have been more limited [43–45].

Within Quantum Materials, the study of quasi one-dimensional (1D) ladders and chains is attractive. In this geometry powerful computational techniques, such as the Density Matrix Renormalization Group (DMRG) [46–49] and Lanczos [16] methods, allow for the theoretical study of model Hamiltonians with considerable accuracy. This removes the veil of theoretical uncertainty in higher dimensional systems that complicates the comparison theory vs experiment. In particular, this 1D avenue may allow the accurate study of systems where *both* topology and correlations are simultaneously relevant, the next grand challenge in Quantum Materials.

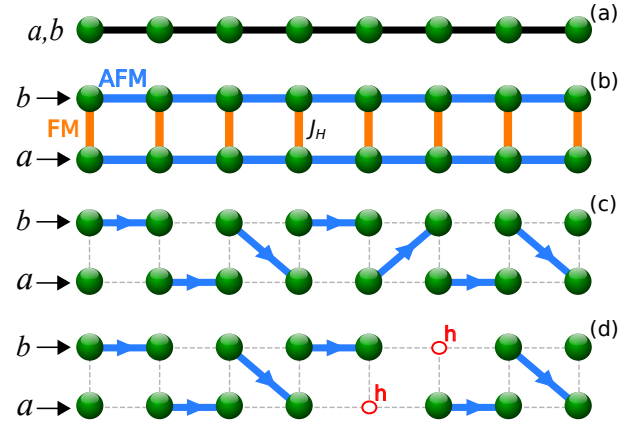


FIG. 1. (a) Sketch of a chain with two active orbitals  $a$  and  $b$ . (b) Representation of panel (a) splitting the orbitals into legs forming a fictitious two-leg ladder, with legs only connected by the Hund coupling  $J_H$ . (c) ORVB state proposed in the text. Arrows indicate spin-1/2 singlets (they are oriented objects) linking NN sites. The full ORVB state is a linear combination of all possible arrangements of these singlets. (d) Doped ORVB state: holes ‘‘h’’ are effectively paired when a preformed electron singlet is removed.

In this context, there are only a few studies of the effects of hole doping and possible magnetic-based hole pairing on topological interacting systems. Early work in the  $t - J$  limit for doped  $S=1$  chains, with double occupancy removed, indicated a narrow region of pairing, suppressed by a competition with ferromagnetism [50]. In related work, triplet superconductivity was also analyzed in 1D [51, 52]. More recent DMRG efforts using multiorbital Hubbard models of interacting electrons unveiled robust tendencies to spin singlet pairing, an ex-

citing result [53, 54]. However, these valuable computational efforts did not provide a concrete mechanism as explanation. In particular, we lack a simple intuitive picture connecting the topological properties of Haldane chains and the emergence of hole pairs in Hubbard models. Developing such a simple “cartoon” may allow generalizations to other systems and also facilitate the experimental search for realizations in particular materials.

The main purpose of our publication is to fill this conceptual gap. Our main conclusion is illustrated in Fig. 1. We provide a new perspective of the two-orbital Hubbard model on a chain, Fig. 1(a), using the two orbitals  $a$  and  $b$  as legs of a mathematically equivalent two-leg ladder, Fig. 1(b). We rely on a hereby proposed ORVB state: the *orbital* generalization of the much discussed resonating valence-bond concepts [55, 56]. We employ preformed spin-1/2 singlets as in the original formulation but now in the enlarged space spanned by the real chain in one direction and the orbital index in another, Fig. 1(c). Doping this state with two holes in principle could break two singlets. But if these holes are close to one another, they can break only one singlet minimizing the energy and leading to an effective *singlet* hole pairing, Fig. 1(d), in agreement with the computational results [53, 54]. The undoped and doped ORVB states are variational, not exact, but they capture the essence of the problem, as shown below.

Our overall conclusions are not obvious: at first sight there are preformed *triplets* at each rung due to the robust  $J_H/U$ . In fact, we predict that triplet pairing – a rarity among superconductors [57–59] – should be stable when easy-plane anisotropies are not negligible. However, doping special quasi-1D materials – with two active fairly equivalent orbitals and weak spin anisotropy – should lead instead to singlet pairing.

## Methods:

**Model** — We use a canonical two-orbital Hubbard model composed of kinetic energy and interaction terms written as  $H = H_K + H_I + H_D$ . The tight-binding portion of the Hamiltonian is

$$H_K = \sum_{i,\sigma,\gamma,\gamma'} t^{\gamma\gamma'} (c_{i\gamma\sigma}^\dagger c_{i+1\gamma'\sigma} + \text{H.c.}), \quad (1)$$

where  $c_{i\gamma\sigma}^\dagger$  ( $c_{i\gamma\sigma}$ ) creates (destroys) an electron at site  $i$  of a chain, orbital  $\gamma$  ( $a$  and  $b$  in our case, although our Hamiltonian notation is generic for arbitrary number of orbitals), and spin projection  $\sigma$ . The nearest-neighbor electron hopping is chosen as a  $2 \times 2$  orbital-space unit-matrix, i.e.  $t^{\gamma\gamma'} = t\delta_{\gamma\gamma'}$ , with  $t$  the energy unit throughout the publication. The non-interacting bandwidth is  $W = 4.0t$ . Note that the hopping symmetry between the two orbitals, and the absence of crystal-field splitting, prevents the appearance of the orbital-selective Mott physics recently studied in related multi-orbital models [60–62].

The electronic interaction is standard:

$$H_I = U \sum_{i,\gamma} n_{i\gamma\uparrow} n_{i\gamma\downarrow} + (U' - \frac{J_H}{2}) \sum_{i,\gamma<\gamma'} n_{i\gamma} n_{i\gamma'} - 2J_H \sum_{i,\gamma<\gamma'} \mathbf{S}_{i\gamma} \cdot \mathbf{S}_{i\gamma'} + J_H \sum_{i,\gamma<\gamma'} (P_{i\gamma}^\dagger P_{i\gamma'} + \text{H.c.}). \quad (2)$$

The first term is the intraorbital Hubbard repulsion  $U$ . The second contains the interorbital repulsion at different orbitals, with the usual relation  $U' = U - 2J_H$  due to rotational invariance. The third term involves the Hund’s coupling  $J_H$ , and the last term represents the on-site interorbital electron-pair hopping ( $P_{i\gamma'} = c_{i\gamma'\uparrow} c_{i\gamma'\downarrow}$ ).

Finally, as shown below, it will also be important to incorporate an easy-plane anisotropy component ( $D > 0$ )

$$H_D = D \sum_i (S_{ia}^z + S_{ib}^z)^2. \quad (3)$$

The spin-1/2 operators  $S^x, S^y, S^z$  are defined using Pauli matrices as  $S_{i\gamma}^\alpha = (1/2) \sum_{\sigma,\sigma'} c_{i\gamma\sigma}^\dagger \sigma_{\sigma,\sigma'}^\alpha c_{i\gamma\sigma'}$ . For our results we used DMRG, with up to  $m = 1800$  states and typical truncation errors below  $10^{-6}$  as in previous investigations [53], as well as the Lanczos method.

## Results:

**Undoped two-orbital Hubbard model at intermediate  $U/W$  vs Haldane state** — Our focus on multi-orbital models originates in iron-based superconductors where ladders and chains can be synthesized, but our results are valid for other transition metal compounds. Iron superconductors are widely believed to be “intermediate” between weak and strong coupling, and  $U/W \sim 1$  is considered realistic [4–7]. Because the iron family is *not* at  $U/W \gg 1$ , a pure spin model is not appropriate and interacting itinerant fermions must be used.

Let us address first whether the model discussed here – with mobile electrons, intermediate  $U/W$ , and hopping unit matrix – is smoothly connected to the Haldane limit. At one particle per orbital and  $U/W \gg 1$  – with concomitant growth of the Hund coupling fixed at the often used ratio  $J_H/U=1/4$  [6, 63, 64] – our model certainly develops S=1 states at every site, antiferromagnetically Heisenberg coupled (we found numerically that the biquadratic coupling, possible in S=1 spin systems, is negligible). To analyze if intermediate  $U/W \sim 1$  and strong coupling  $U/W \gg 1$  (with S=1 spins onsite) are qualitatively similar, we compute with DMRG the *entanglement spectra* ES [66]. For example, working at  $U/W = 1.6$ , where hole-binding is maximized as shown below, Figs. 2(a,b) indicate that with increasing  $J_H/U$  the Hubbard ES clearly resembles the S=1 chain ES [67].

However, our model is not merely a S=1 chain. For example, the inset of Fig. 2(c) indicates that the von Neumann entropy [68–70]  $S_{VN}$  (see Appendix A.1) converges to  $\ln(2)$  (S=1 chain result) only at  $U/W \sim 5$  and beyond. At typical couplings of iron compounds,  $S_{VN}$  is approximately double the  $U/W \gg 1$  limit. Thus, the

two-orbital Hubbard model qualitatively does resemble the Haldane chain, but at  $U/W \sim 1$  there are quantitative differences likely caused by non-negligible charge fluctuations.

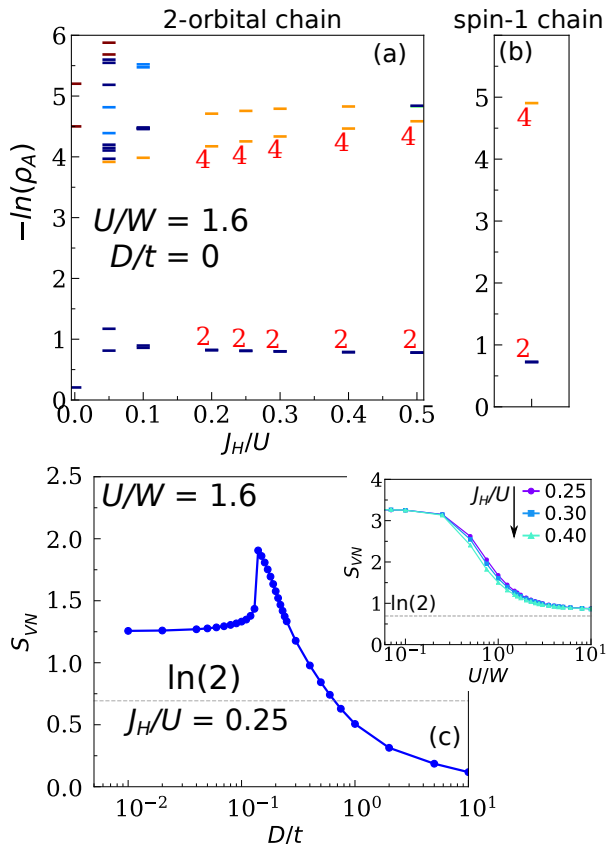


FIG. 2. Entanglement spectra for: (a) the undoped two-orbital Hubbard chain vs  $J_H/U$ , at fixed  $U/W = 1.6$ , and (b) the  $S=1$  Heisenberg chain (both at  $D/t = 0$ ). At robust  $J_H/U$  in (a), a two-fold degeneracy is clear in both cases. (c) Von Neumann entanglement entropy ( $S_{VN}$ ) for the undoped two orbital-chain model vs  $D/t$ , at  $U/W = 1.6$  and  $J_H/U = 0.25$ . *Inset*:  $S_{VN}$  vs  $U/W$  for  $D/t = 0$  and various  $J_H/U$ s showing convergence to the expected  $\ln(2)$  of the  $S=1$  chain at  $U/W \gg 1$ . The DMRG results in (a-c) use OBC  $N = 100$  sites, both for Hubbard and Heisenberg  $S=1$  models.

Consider now how the model evolves with increasing anisotropy  $D/t$ . Recent work found a transition between the gapped Haldane region and a gapped state with trivial topology [54]. In Fig. 2(c) indeed  $S_{VN}$  at fixed  $U/W = 1.6$  and  $J_H/U = 0.25$  does *not* evolve smoothly from  $D/t = 0$  – connected to the Haldane limit at large  $U/W$  – to the anisotropic large  $D/t$  “XY” limit. The ground state in this limit has a spin triplet with  $S^z = 0$  projection at every site, and no edge states. At  $0.1 < D/t < 0.2$ , an abrupt change occurs and eventually  $S_{VN} \rightarrow \ln(1)$  as  $D/t$  grows, compatible with a product state of  $S^z = 0$  triplets [see discussion later, Eq.(4)].

In summary, although with quantitative differences, the undoped Hubbard model qualitatively resembles the

Haldane chain. This occurs as long as  $D/t$  does not cross a threshold beyond which edge states disappear and a topologically trivial regime develops.

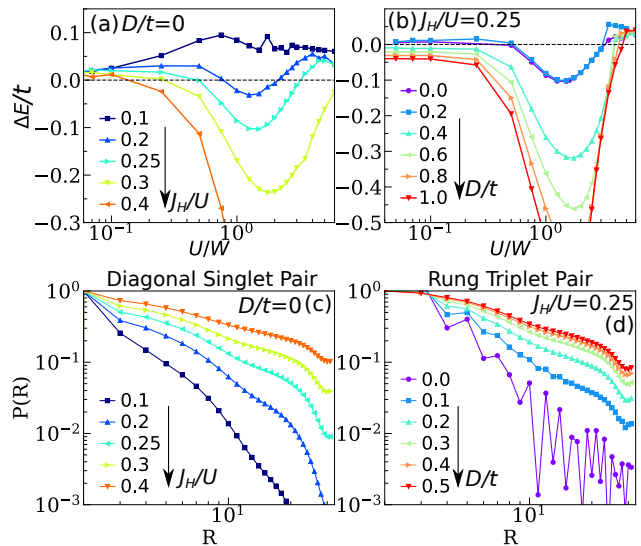


FIG. 3. Binding energy  $\Delta E/t$  vs  $U/W$  for various values of (a)  $J_H/U$ , at fixed  $D/t = 0$ , and (b)  $D/t$ , at fixed  $J_H/U = 0.25$ . In (a,b), a 16-sites OBC chain was used and DMRG. (c) Spin-singlet  $\Delta_S$  real-space pair-pair correlations  $P(R)$  vs distance  $R$ , varying  $J_H/U$ , at fixed  $U/W = 1.6$  and  $D/t = 0$ .  $\Delta_S$  involves NN sites and different orbitals. (d) Same as (c) but using the rung triplet operator  $\Delta_T$ , varying  $D/t$ , at fixed  $U/W = 1.6$  and  $J_H/U = 0.25$ . In (c,d), a 48-sites OBC chain was used and DMRG, neglecting 8 sites at each end to avoid edge effects. Correlations are normalized to the result at distance 2,  $P(2)$ , to better focus on the large  $R$  behavior. For definition of  $\Delta_S$  and  $\Delta_T$ , see Appendix A.2. At (c) the hole doping is  $x = 0.042$  corresponding to 4 holes, while at (d)  $x = 0.083$  corresponding to 8 holes.  $x$  is defined as number of holes divided by 96 (48 sites, 2 orbitals).

**Pairing in the doped two-orbital Hubbard model** — The main focus of this publication is why pairing occurs and why in the channel it occurs. However, before addressing these issues, let us first review and extend recent DMRG studies about hole pair formation and pair-pair correlations in the doped two-orbital Hubbard model. This analysis will provide hints for the intuitive explanation. In Fig. 3(a) the 2-holes binding energy vs  $U/W$  is shown, parametric with  $J_H/U$ . This binding energy is defined as  $\Delta E = E(2) - E(0) - 2[E(1) - E(0)]$ , where  $E(M)$  is the ground state energy with  $M$  holes (zero holes refers to the half-filled state with one electron per orbital). When  $\Delta E$  becomes negative, it signals a 2-holes bound state. Clearly, Fig. 3(a) indicates pair formation with maximum  $|\Delta E|$  at  $1 < U/W < 2$ , as in [53], and growing with increasing  $J_H/U$  (note  $J_H/U$  should be less than  $1/3$  to remain smaller than  $U'/U$  due to the constraint  $U' = U - 2J_H$ ). At  $U/W \gg 1$ , ferromagnetism for 1 and 2 holes – see discussion below – prevents pairing

suggesting that directly doping the S=1 chain may not be the proper theoretical approach. In Fig. 3(b) we show new results, now increasing  $D/t$  at fixed  $J_H/U = 0.25$ . Robust pairing tendencies are observed again. However, the binding curves are almost identical at  $D/t = 0.0$  and  $0.2$ , but then they rapidly increase in magnitude. This reflects *qualitative* differences in the pairing properties, compatible with the von Neumann analysis with increasing  $D/t$  in Fig. 2(c) that indicated a topological change in the same  $D/t$  range.

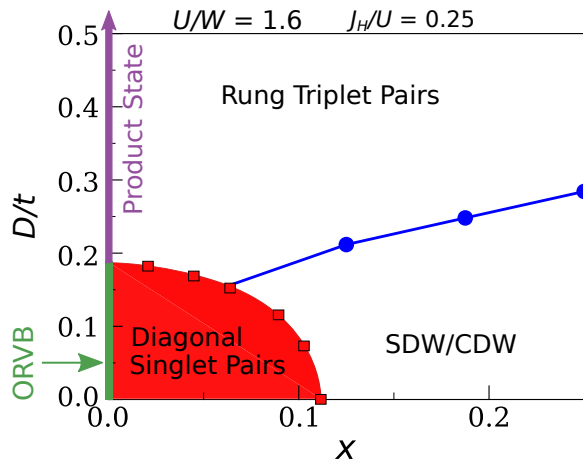


FIG. 4. Qualitative phase diagram varying the easy-plane anisotropy  $D/t$  and hole doping  $x$ , at fixed  $U/W = 1.6$  and  $J_H/U = 0.25$ , using DMRG. Hole density  $x = 0$  represents half-filling where at  $D/t \gtrsim 0.2$  the ground state is qualitatively connected to the S=1 Haldane phase. “ORVB” refers to the variational state introduced later in the text. At larger  $D/t$ , a product state of rung triplets with zero spin projection Eq.(4) is a good representation of the ground state. Upon doping at small  $D/t$ , first singlet pairing dominates until at  $x \sim 0.1$  the spin/charge density wave (SDW/CDW) correlations – not shown – become stronger. Doping of the product state ( $D/t \gtrsim 0.2$ ) leads to spin-triplet rung pairing over a broad range of doping because the natural “preformed” Cooper pairs are rung triplets. We used DMRG and  $N = 48$  OBC chains to construct the phase diagram. Only a few points are shown with dots, but a denser grid ( $x, D/t$ ) was analyzed via DMRG.

The qualitative transition in Fig. 3(b) also occurs in Figs. 3(c,d) where pairing correlations are shown. At  $D/t = 0$  and  $J_H/U = 0.25$ , when doping a region smoothly connected to the Haldane chain, spin-*singlet* pairing dominates (while triplet is exponentially suppressed, not shown). With increasing  $D/t$  at fixed hole density  $x$ , a transition from singlet to triplet dominance is observed. For example, in panel (d) we observe that spin-triplet pairing, heavily suppressed at  $D/t = 0$ , instead becomes dominant as  $D/t$  increases (while singlet is exponentially suppressed, not shown).

The “global summary” is shown in Fig. 4, where a large set of DMRG data is summarized in a phase diagram varying  $D/t$  and doping  $x$ , with just a few representative points displayed. The red region near  $x = 0$

and  $D/t = 0$  is where the model resembles the Haldane state according to the entropy entanglement. Here, at light doping  $x$  singlet-pairing dominates at intermediate  $U/W$ , but eventually other non-superconducting channels (SDW and CDW) take over at larger  $x$ . Increasing  $D/t$ , at small  $x$  a transition from singlet- to triplet-dominated pairing occurs. In the singlet regime, holes are primarily located at nearest-neighbor sites and different orbitals, while in the triplet regime they are primarily at the same rung also in different orbitals.

The DMRG results unveiled a region of parameter space (small  $D/t$ , low hole doping, intermediate  $U/W$ , robust  $J_H/U$ ) where superconducting spin-singlet correlations dominate. These results are surprising. First, the connection with the S=1 chain suggests that antiferromagnetic (AFM) fluctuations are short-range and it is unclear if they are sufficiently strong to generate pairing. Second, at every site and at intermediate-strong  $U/W$  a nonzero magnetic moment develops due to  $J_H$ . Naively, these same-site electrons can be considered as local “preformed” triplets. Then, after hole doping the resulting ground state could be envisioned as involving these triplets that became mobile. For  $D/t > 0.2$ , Fig. 4, this naive perspective is confirmed numerically. Rung spin-triplet pairing dominates, and the product state wave function Eq.(4) is a good variational approximation (undoped system) which becomes exact as  $D \rightarrow \infty$ :

$$|TPS\rangle = \prod_i^N |1, 0\rangle_i = \prod_i^N \frac{1}{\sqrt{2}} (|\uparrow_{ia}\downarrow_{ib}\rangle + |\downarrow_{ia}\uparrow_{ib}\rangle). \quad (4)$$

Then, what originates the singlet dominance at small  $D/t$ ? Although in a Haldane regime all triplet correlations must decay exponentially, such reasoning does not explain why singlet pairing is enhanced. Hints for the ORVB explanation presented below arise from the Affleck-Kennedy-Lieb-Tasaki (AKLT) exact solution [3], where a S=1 spin model was considered employing two auxiliary idealized S=1/2 degrees of freedom at every site. These auxiliary states form spin singlets with other S=1/2 auxiliary states at the next site. Below, we show that our two-orbital Hubbard model shares properties similar to this idea.

#### ORVB state for the two-orbital Hubbard chain

— Here we introduce a variational state for both the undoped and lightly doped two-orbital Hubbard chain, at intermediate and strong  $U/W$ . We argue that these ground states can be qualitatively described in terms of S=1/2 spin singlets involving NN sites, connecting the same or different orbitals. *Our main result is that the small  $D/t$  region of the two-orbital Hubbard model has hidden “preformed” singlets that become mobile with doping.* Knowing what type of Hubbard model develops pairing, and specifically what type of hoppings, allow us to formulate predictions on what characteristics a material must display to realize this physics.

We will propose a variational state inspired by an exact equality. Consider first only 2 sites, say 1 and 2, and construct the quantum global spin-zero state using one electron per orbital. With only one orbital this has the canonical expression  $|Singlet_{S=1/2, 2\text{-sites}}\rangle = \frac{1}{\sqrt{2}}(|1/2, 1/2\rangle_1 |1/2, -1/2\rangle_2 - |1/2, -1/2\rangle_1 |1/2, 1/2\rangle_2) = \frac{1}{\sqrt{2}}(|\uparrow_1\downarrow_2\rangle - |\downarrow_1\uparrow_2\rangle)$ , where,  $|1/2, 1/2\rangle$  means total spin  $1/2$  and  $z$ -projection  $\uparrow$ , etc.

For two spins 1, the global spin zero state is still relatively simple

$$|Singlet_{S=1, 2\text{-sites}}\rangle = \frac{1}{\sqrt{3}}(|1, 1\rangle_1 |1, -1\rangle_2 + |1, -1\rangle_1 |1, 1\rangle_2 - |1, 0\rangle_1 |1, 0\rangle_2). \quad (5)$$

Because in our case each site  $S=1$  arises from two real  $S=1/2$  electrons at each orbital and the same site, we use the notation  $|1, 1\rangle_1 = |\uparrow_{1,a}\uparrow_{1,b}\rangle$ ,  $|1, -1\rangle_1 = |\downarrow_{1,a}\downarrow_{1,b}\rangle$ ,  $|1, 0\rangle_1 = \frac{1}{\sqrt{2}}(|\uparrow_{1,a}\downarrow_{1,b}\rangle + |\downarrow_{1,a}\uparrow_{1,b}\rangle)$ , and an analogous expression at site 2. Then, simple algebra leads to

$$\begin{aligned} |Singlet_{S=1, 2\text{-sites}}\rangle &= \\ &= \frac{1}{\sqrt{3}}(|\uparrow_{1,a}\uparrow_{1,b}\downarrow_{2,a}\downarrow_{2,b}\rangle + |\downarrow_{1,a}\downarrow_{1,b}\uparrow_{2,a}\uparrow_{2,b}\rangle) \\ &- \frac{1}{2\sqrt{3}}(|\downarrow_{1,a}\uparrow_{1,b}\uparrow_{2,a}\downarrow_{2,b}\rangle + |\uparrow_{1,a}\downarrow_{1,b}\downarrow_{2,a}\uparrow_{2,b}\rangle \\ &+ |\uparrow_{1,a}\downarrow_{1,b}\uparrow_{2,a}\downarrow_{2,b}\rangle + |\downarrow_{1,a}\uparrow_{1,b}\downarrow_{2,a}\uparrow_{2,b}\rangle). \end{aligned} \quad (6)$$

What is remarkable is that this last expression can be *exactly* rewritten as a combination of  $S=1/2$  singlets, involving either different or the same orbitals:

$$\begin{aligned} |Singlet_{S=1, 2\text{-sites}}\rangle &= \frac{-1}{\sqrt{3}} [ \\ &\frac{1}{\sqrt{2}}(|\uparrow_{1,a}\downarrow_{2,b} - \downarrow_{1,a}\uparrow_{2,b}\rangle) \frac{1}{\sqrt{2}}(|\uparrow_{1,b}\downarrow_{2,a} - \downarrow_{1,b}\uparrow_{2,a}\rangle) - \\ &\frac{1}{\sqrt{2}}(|\uparrow_{1,a}\downarrow_{2,a} - \downarrow_{1,a}\uparrow_{2,a}\rangle) \frac{1}{\sqrt{2}}(|\uparrow_{1,b}\downarrow_{2,b} - \downarrow_{1,b}\uparrow_{2,b}\rangle) ]. \end{aligned} \quad (7)$$

Much intuition is gained when this exact mathematical result is represented visually, as in Fig. 5, where we have rewritten exactly Eq.(7) doubling the number of valence-bonds states for an easier extrapolation to more sites.

Our exact result is counterintuitive: with perfect  $S=1$  states at each site, the total spin-zero state of the two-orbital two-sites Hubbard model can be represented exactly as a linear combination of  $S=1/2$  singlets. This is qualitatively in agreement with the AKLT perspective [3]. Our result Eq.(7) leads to our conjecture that a “hidden”  $S=1/2$  orbital-resonating-valence-bond state emerges. Figure 5 resembles the original views of Anderson, Affleck *et al.*, but now with orbitals considered as legs of a two-leg ladder, with these legs only connected by the Hund coupling (no interleg hopping).

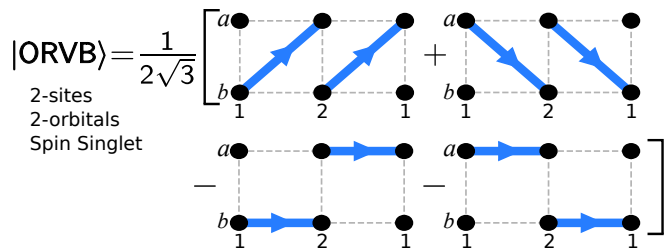


FIG. 5. Normalized-to-one two-site two-orbital undoped ground state of the Hubbard model at large  $U/W$ , Eq.(7), when double occupancy is neglected. Shown is the total spin zero state of two sites, with two electrons per site, represented exactly in terms of  $S=1/2$  singlets (shown as oriented blue arrows).  $a$  and  $b$  are the two orbitals and  $(1,2)$  are the sites. Results are depicted as with periodic boundary conditions (PBC), providing a natural extension beyond two sites, leading to our proposed ORVB variational state below.

Then, intuitively, the undoped state has preformed  $S=1/2$  singlet pairs, in all possible arrangements, that upon doping can become mobile, leading to the dominance of spin-singlet pairing. Thus, we predict that doping real quasi-one-dimensional materials represented by two nearly-degenerate orbitals should lead to superconductivity in the spin-singlet channel if anisotropies are not large. We need two “similar” orbitals because we used a  $2\times 2$  unit hopping matrix. If XY-like anisotropies become robust, then the also exotic triplet-channel should dominate, as shown below.

How can this be generalized to more sites? The two-sites exact result in Fig. 5 assuming PBC clarifies this matter. The rule is that in each elementary  $2\times 2$  plaquette only *one* singlet can be used, either along a diagonal or along a leg. Each ladder site with a  $S=1/2$  degree of freedom can be used only once: after they form a singlet they disappear from the picture. Moreover, the two sites example has other properties common to a longer chain. The 2-sites ORVB state is *even* under the exchange of orbitals  $a$  and  $b$  and also even under a reflection with respect to the middle of the plaquette. Now the extension to more sites becomes natural. For example, in Fig. 6 we show the 16 ORVB states needed for 4 sites using PBC, as well as the “representative” of each class (i.e. applying to a representative translations and orbital exchange, the full original class can be reconstructed). We remark again that, by construction, the ORVB states have perfect  $S=1$  spins at every site in spite of using spin- $1/2$  singlets as building blocks.

**Lanczos overlaps** — How accurate is this state? Using Lanczos, we calculated the normalized exact ground state  $|GS\rangle$  of the two-orbital Hubbard model in short chains and computed the overlap with a linear combination of the individual ORVB states of Fig. 6. The coefficients for each class were optimized to maximize the global overlap, arriving to a final normalized-to-one

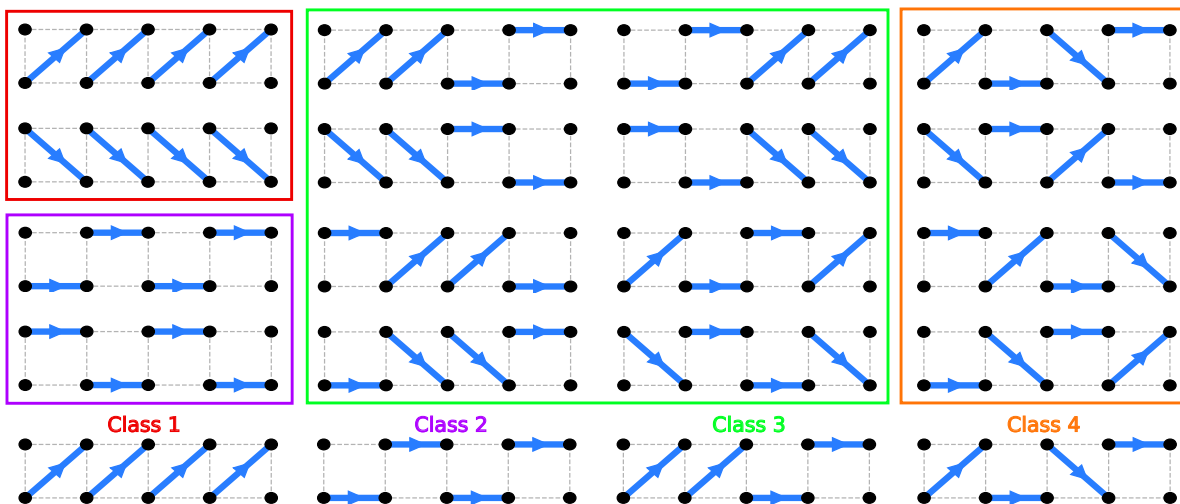


FIG. 6. Individual ORVB states for the four-sites half-filled two-orbital Hubbard model with PBC. The color-framed states represent 4 distinct “classes”. A representative of each class is shown at the bottom with the same color convention. By applying translation and orbital exchange for each representative (reflection is not needed for the undoped case), we recover all the rest of the states shown in the upper frames. Note that the 16 ORVB states displayed are *not* orthogonal to one another.

state dubbed  $|ORVB\rangle$ . Care must be taken because the individual ORVB components do not form an orthogonal set since their overlap is finite. By this procedure, at  $U/W = 20$  and 2 sites, the overlap  $|\langle ORVB|GS\rangle|$  is virtually 1, because double occupancy is nearly entirely suppressed, as in Eq.(7). Using 4 sites, the binding energy is now optimized at  $U/W = 4$ . At this coupling and size, we found  $|\langle ORVB|GS\rangle| = 0.95$  indicating that  $|ORVB\rangle$  is a good representation of the ground state.

We carried out extensions to more sites using PBC. As already explained, below when “classes” are mentioned for the undoped case, they represent groups of ORVB states related by applying translations and orbital exchange to a particular representative. For 6 sites, there are 8 classes and at  $U/W = 2$ , where binding is maximized (not shown), the overlap is 0.79. As the lattice size grows, other configurations involving longer  $S=1/2$  singlets and specially doubly occupied orbitals will contribute to the ground state because the optimal  $U/W$  where binding is maximized is reduced reaching the intermediate range. But finding a robust 0.79 overlap with 6 sites indicates that  $|ORVB\rangle$  is a good variational state. The same occurs for 8 sites: here the number of classes grows to 16, and when  $U/W = 1.5$  is chosen because it optimizes the binding energy, the overlap  $|\langle ORVB|GS\rangle|$  for 8 sites remains robust at 0.61. As the system continues increasing in size, the optimal binding converges to intermediate  $U/W$ , see Fig. 3.

Should we worry about a reducing overlap with increasing size? As example consider the simple  $(\pi, \pi)$  spin staggered state  $|stagg\rangle = |\uparrow\downarrow\uparrow\dots\rangle$  of the  $S=1/2$  Heisenberg model two-dimensional square lattice. For a  $2\times 2$  cluster its overlap with the true ground state is 0.58 but for the  $4\times 4$  cluster it decreases to 0.29. However,  $|stagg\rangle$  is certainly a good “variational state”. A reducing over-

lap is natural because with increasing cluster size the fraction of the total Hilbert space spanned by simplified variational states – ORVB for two-orbital Hubbard, spin staggered for Heisenberg, etc. – rapidly decreases. Thus, after confirming the overlap is robust for small clusters, what matters more is whether the proposed state captures the essence of the ground state, as shown next.

**Doped ORVB** — Now let us generalize the variational ORVB state to the doped case, to our knowledge a topic barely addressed in the resonating valence-bond context. In our DMRG studies in Fig. 3 and in previous efforts [53], we found that in the 2-holes ground state the largest-weight configuration occurs when holes are placed at NN sites and in different orbitals. Having the two holes in the same leg is not optimal because it leads to collisions: with one hole per leg they can move without obstacles, while taking advantage of the effective attraction in the ORVB arrangement. For this reason, and to reduce complexity, our proposed doped ORVB state will have only one hole per orbital and will be obtained primarily by taking the undoped ORVB and *removing one diagonal singlet*. This is exemplified for 4-sites PBC in Fig. 7 (left) where classes are shown. Note that the diagonal character of the  $2\times 2$  hopping matrix establishes that the number of holes per orbital is conserved.

However, two extra ingredients are needed for a proper physical description. First, quantum mechanically each hole in each orbital is “oscillating” (zero-point motion) via the intraorbital hopping because these are not frozen holes. Then, the configuration with 2 holes in the same rung must be included because it is generated in that oscillation within the bound state. Second, to avoid having unpaired  $S=1/2$  electrons left and right of that 2-holes rung, a singlet across is required, as shown on the three

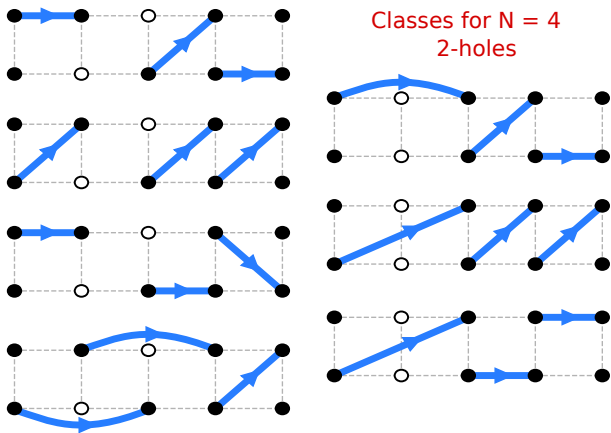


FIG. 7. A representative of each of the 7 ORVB classes used for a 4-sites chain with PBC and 2-holes doping. Each class state represents a linear combination involving translated, orbital  $a \leftrightarrow b$  exchanged, and parity-inverted states.

classes in Fig. 7 (right). Indeed it is known that a “ $\pi$ -shift” across-the-hole develops in the spin correlations of the two-orbital Hubbard ground state [53]. This also occurs in one-orbital  $t-J$  models [71, 72]. For completeness, singlets across-the-hole were also added for diagonal hole configurations as in the bottom left class of Fig. 7.

This procedure resembles qualitatively the exact solution of the  $U = \infty$  single-orbital Hubbard chain [73]: holes and spins are independent in this limit. Our mobile holes can be visualized as *effectively inserted in between the original singlets of the undoped ORVB state*.

The  $|ORVB\rangle$  state generalized from Fig. 7 but now for 6 sites and 2 holes requires 23 classes [for 2 holes, to generate all states not only translational symmetry and exchange of orbitals must be used, but also reflection (parity) with respect to the middle]. The overlap with the 2-holes Lanczos exact GS at  $U/W = 2$  is 0.59. For 8 sites and 2 holes, 84 classes are needed, and the overlap at  $U/W = 1.5$  is 0.48. These are good numbers, but more important is how *qualitatively* these states capture the essence of the problem. For instance, from the 6-sites exact GS the spin-spin correlations can be measured using special operators to project [53, 74] the mobile holes to their highest-probability ground state position [38, 53]. The Lanczos and ORVB variational results are contrasted in Figs. 8 (a,b). The agreement is remarkable. While away from the holes the pattern resembles the undoped case, with ferromagnetic (FM) rungs and AFM legs [53], near the hole the AFM correlation “across-the-hole”, typical of carriers in an AFM background, is reproduced. Moreover, the *a priori puzzling* FM link diagonally placed opposite to the diagonal of holes is also observed. Naively this may suggest that triplets are needed in the undoped variational state along diagonals. However, this effective FM correlation is merely a consequence of the mobility of the holes that displace the original on-site rung FM triplet, contained in the ORVB state by construction, from rung to diagonal.

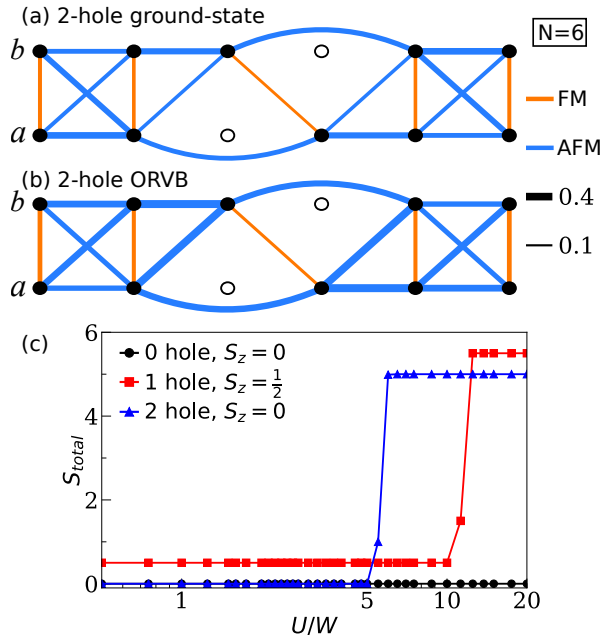


FIG. 8. Schematic of the real-space spin-spin correlations in the two-orbital chain for (a) the 2-holes exact ground-state and (b) the 2-holes ORVB state. The lower (upper) chain represents the orbital  $a$  ( $b$ ). The holes, which are of course mobile, are projected to their most likely position in the state via projector operators [53, 74], and then spin-spin correlations are measured. Blue (red) lines represent AFM (FM) bonds with line-thickness proportional to the magnitude of spin correlations. (c) Total ground-state spin quantum number vs  $U/W$ , for 0, 1, and 2 holes. All calculations (a,b,c) are performed using Lanczos on a 6-sites PBC chain, at  $U/W = 2.0$ ,  $J_H/U = 0.25$ , and  $D/t = 0$ .

Panel Fig. 8 (c) also shows that at very large  $U/W$  the pairing and overall proposed picture breaks down. In this regime, the Hund coupling is so large that “double-exchange” physics dominates and the system turns globally ferromagnetic to improve the kinetic energy of the now unbounded holes. This shows that simply doping the  $S=1$  Haldane chain may not be a proper path, but  $U/W$  must be reduced to intermediate values to avoid the ferromagnetic competition. However, in the hole-binding range the total spin quantum numbers are qualitatively compatible with those of the ORVB picture.

**Varying  $D/t$**  — When easy-plane anisotropies are included, the spin-triplets product state at each rung,  $|TPS\rangle$  Eq.(4), becomes increasingly a better approximation as  $D/t$  grows (at  $D/t \rightarrow \infty$ ,  $|TPS\rangle$  is the exact ground state). This evolution is illustrated in Fig. 9. In (a), the half-filling overlaps  $|\langle ORVB|GS\rangle|$  and  $|\langle TPS|GS\rangle|$  are shown. The ORVB (TPS) overlap decreases (increases) with increasing  $D/t$ , as expected. Note that the TPS state used here is crude: larger overlaps in the  $D/t$  range shown could be obtained adding fluctuations but this is irrelevant for our main focus i.e. the origin of the spin-singlet pairing at small  $D/t$ .

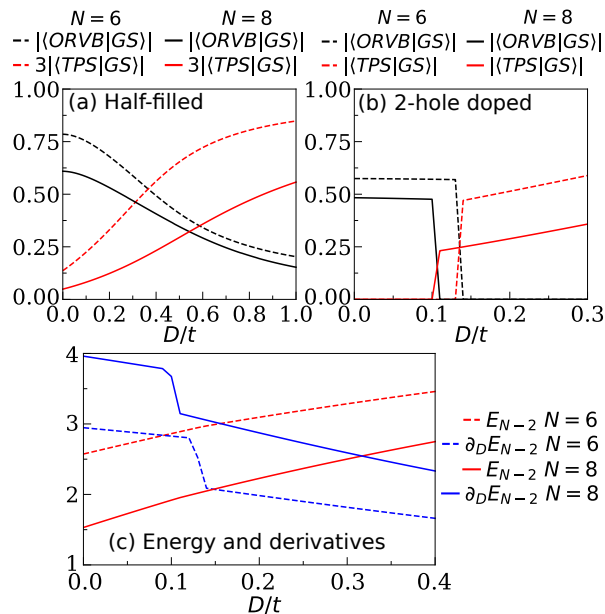


FIG. 9. Overlap  $|\langle ORVB|GS\rangle|$  and  $|\langle TPS|GS\rangle|$  vs  $D/t$  for (a) zero hole (half-filling) and (b) two holes. The discontinuity in (b) indicates a first-order transition due to a level crossing and associated change in the ground state quantum numbers under orbital exchange. (c) Ground-state chain energies, as well as their derivatives to emphasize sudden slope changes, for two holes  $E_{N-2}$ . All results (a-c) obtained with Lanczos using  $N = 6$  and 8 sites and PBC.

In addition, we observed that the spin-spin correlations involving the  $z$  components within the two orbitals of the same rung correctly evolve with increasing  $D/t$  (not shown). At small  $D/t$ , they are FM because a full vector spin close to magnitude  $S=1$  forms at each site. At large  $D/t$ , they become AFM because only the  $|1,0\rangle$  component survives in the XY product state. Also note the  $|ORVB\rangle$  and  $|TPS\rangle$  states are not orthogonal to one another, but their overlap is very small (0.02 for  $N = 8$ , 0.07 for  $N = 6$ , both at  $D = 0$  PBC).

The case of 2 holes, panel (b), is more interesting. Here a *level crossing* occurs [panel (c)]: at small  $D/t$  the 2-hole-doped  $|ORVB\rangle$  has a nonzero overlap with  $|GS\rangle$  because both states have quantum number  $(-1)$  under orbital exchange (“orbital antisymmetric”). However, at  $D/t \sim 0.125$  – where the von Neumann entropy Fig. 2(c) signaled a qualitative transition in the undoped case – a level crossing occurs in the Lanczos ground state. At large  $D/t$  the quantum number under orbital exchange becomes  $(+1)$  leading to a nonzero overlap with the “orbital symmetric” 2-hole  $|TPS\rangle$  state.

**Conclusions** — We introduced an Orbital Resonant Valence Bond variational state for the undoped and hole-doped two-orbital Hubbard chain, and predict the development of spin-singlet pairing upon doping. Our state is qualitatively similar to the resonant valence-bond states of Anderson, Affleck, *et al.*, but in an extended ladder-like geometry spanned by the real chain in the long axis

and the number of orbitals in the short axis. Using DMRG and Lanczos, we find excellent agreement with the ORVB predictions at intermediate  $U/W$ . The entanglement spectra and von Neuman entropy indicate that the undoped intermediate  $U/W$  regime is analytically connected to the Haldane limit at  $U/W \gg 1$ . However, in the realm of spin models at  $U/W \gg 1$ , a strong competition with ferromagnetism upon doping prevents pairing from occurring.

Our ORVB state relies on a mathematical expression involving two  $S=1$  spins at NN sites, with one electron per orbital. The global spin-zero state of these two sites is written *exactly* exclusively using spin-1/2 singlets linking electrons at those NN sites, involving the same or different orbitals. Extended to more sites, the ORVB state is a linear combination of spin-1/2 singlets in all possible NN arrangements. Note that same-rung singlets are excluded because of the large ferromagnetic Hund coupling. Using Lanczos on finite chains, the ORVB was shown to be a good approximation to the true ground state for small easy-plane anisotropy  $D/t$ , robust Hund coupling  $J_H/U$ , intermediate  $U/W$ , and light hole doping.

The preformed NN spin singlets – resembling Cooper pairs – become mobile upon hole doping, and form a coherent superconducting state, at least within the limitations of one dimensionality that only allow for power-law decays. A weak coupling among chains will render the state truly superconducting with long-range order, as in two-leg Cu- or Fe-based ladders. Our results explain the unexpected spin-singlet dominance observed computationally in a regime that naively contains preformed on-site rung triplets. These triplets indeed do condense into a triplet superconductor but only increasing  $D/t$  beyond a finite threshold. This is also an exotic state since triplet superconductivity is rare.

In summary, our study combines topological concepts with correlation effects. Pairing emerges with hole doping via the liberation of preformed spin-1/2 singlets already contained in the undoped ORVB state. For experimentalists to realize our model the challenge is to find quasi-1D materials with two nearly-degenerate dominant active orbitals, and with similar overlaps along the chain so that the hopping matrix is nearly the unit matrix, as in our calculations. How robust the Haldane regime is with regards to small deviations from this hopping symmetric case, as well as the introduction of an orbital small crystal-field splitting, remain to be investigated (the orbital-selective Mott phase is close in parameter space, as recently shown [60–62]). Doping the existing physical realizations of undoped Haldane chains [8–12] can provide a starting point towards the predicted superconductivity, but again we remark that intermediate  $U/W$  is a more attractive parameter region than  $U/W \gg 1$ . For this reason the iron-superconductors family provides a natural starting point, although realizations could also be found in other multiorbital-active compounds.

## Appendix:

**A.1 Entropy** — In the main text, we present calculations of the entanglement spectrum and the Von Neumann entanglement entropy. These results are obtained by creating a bipartite system, as naturally occurs in the DMRG algorithm. Labeling these partitions  $A$  and  $B$ , one can calculate the density matrix of sub-system  $A$  by tracing over the  $B$  sub-section of the full density matrix, defining the reduced density matrix  $\rho_A = \text{tr}_B(|\Psi_0\rangle\langle\Psi_0|)$ . Finally, using the eigenvalues of  $\rho_A$ , the von Neumann entanglement entropy can be defined

$$\begin{aligned} S_{VN} &= -\text{Tr}[\rho_A \ln(\rho_A)] \\ &= -\sum_i \rho_{ii}^A \ln(\rho_{ii}^A) \quad \text{in the diagonal representation.} \end{aligned} \quad (8)$$

It is well known that the eigenvalues of the ground-state reduced density matrix of a generic bipartition of the lattice correspond to the squares of the singular values of a Schmidt decomposition of the many-body wave-function written as a matrix product state [47]. These singular values represent the correlations or entanglement between sub-systems  $A$  and  $B$ . Therefore, the spectrum of singular values is referred to as the entanglement spectrum ( $\text{ES} = -\ln(\rho_A)$ ). Phases with short-range correlation length (gapped) have lower  $S_{VN}$  compared to gapless phases with larger correlation length. To this end,  $S_{VN}$  and the singular values also provide an easy way to probe phase transitions. These quantities are extensively used to probe topological phases where notions of local order parameters break down, leading to constraints where one must use non-local quantities such as entanglement. For example, quantum spin liquids are defined as a phase of matter where spins remain disordered even at zero temperature while retaining long-range entanglement. In addition, topological phases of matter often leads to edge states that can also be probed using the entanglement spectrum (ES). In the main text, we compare the ES of our model with that of an AFM spin-1 Heisenberg model whose ground state is characterized by having edge states (Haldane phase) leading to a two-fold degeneracy in the ES. By comparison, we showed that the ground state of a two-orbital chain with large Hund's coupling  $J_H/U$  and Hubbard repulsion  $U/W$  leads to the Haldane phase.

**A.2 Operators** — To address pairing, we defined a general pair creation operator as

$$\Delta_{(i,j),\pm}^{\gamma\gamma'} \dagger = \frac{1}{\sqrt{2}}(c_{i,\gamma,\uparrow}^\dagger c_{j,\gamma',\downarrow}^\dagger \pm c_{i,\gamma,\downarrow}^\dagger c_{j,\gamma',\uparrow}^\dagger), \quad (9)$$

where  $i, j$  are sites,  $\gamma, \gamma'$  are orbitals ( $a$  or  $b$ ), and  $\pm$  sign represents a spin singlet or triplet. We only focused on two different pair operators: (1) nearest neighbor pair that is odd

under spin (singlet) and under orbital exchange ( $S_{nn}^\dagger$  below), (2) on-site inter-orbital pair that is even under spin (triplet) and under orbital exchange ( $T_{on}^\dagger$ ). These are defined as

$$\begin{aligned} \Delta_S &= S_{nn}^\dagger(i) = \Delta_{(i,i+1),-}^{ab\dagger} - \Delta_{(i,i+1),-}^{ba\dagger} \\ \Delta_T &= T_{on}^\dagger(i) = \Delta_{(i,i),+}^{ab\dagger} \end{aligned} \quad (10)$$

In the main text, we often refer to  $S_{nn}^\dagger$  as odd diagonal singlet and to  $T_{on}^\dagger$  as rung triplet, where ‘‘diagonal’’ and ‘‘rung’’ refers to the ladder representation of a two-orbital chain Fig. 1. Using these pair creation operators, we study the decay of the pair-pair correlations

$$\begin{aligned} P_S(R) &= \frac{1}{N_R} \sum_i \langle S_{nn}^\dagger(i) S_{nn}(i+R) \rangle, \\ P_T(R) &= \frac{1}{N_R} \sum_i \langle T_{on}^\dagger(i) T_{on}(i+R) \rangle, \end{aligned} \quad (11)$$

where  $N_R$  represents the number of total neighbors at distance  $R$  with respect to site  $i$ , summed over all sites.

**Code and Data Availability** — The computer codes used in this study are available at <https://g1257.github.io/dmrgPlusPlus/>. The data that support the findings of this study are available from the corresponding author upon request.

**Acknowledgments** — We thank A. Moreo for useful discussions. N. D. P., N. K., A. N., and E. D. were supported by the U.S. Department of Energy (DOE), Office of Science, Basic Energy Sciences (BES), Materials Science and Engineering Division. G. A. was supported by the Scientific Discovery through Advanced Computing (SciDAC) program funded by the U.S. Department of Energy, Office of Science, Advanced Scientific Computing Research and Basic Energy Sciences, Division of Materials Sciences and Engineering. Part of this work was conducted at the Center for Nanophase Materials Sciences, sponsored by the Scientific User Facilities Division (SUFD), BES, DOE, under contract with UT-Battelle.

**Author contributions** — N. D. Patel and E. Dagotto planned the project and provided insight into the understanding of the spin singlet pairing mechanism. N. D. Patel and N. Kaushal performed all the calculations for the multi-orbital Hubbard model. A. Nocera and G. Alvarez developed the DMRG++ computer program.

**Competing interests** — The authors declare no competing interests.

\* Corresponding author. Email: edagotto@utk.edu

<sup>1</sup> Hasan, M. Z. & Kane, C. L. Colloquium: Topological insulators. *Rev. Mod. Phys.* **82**, 3045 (2010). <https://doi.org/10.1103/RevModPhys.82.3045>

<sup>2</sup> Haldane, F. D. M. Nonlinear Field Theory of Large-Spin Heisenberg Antiferromagnets: Semiclassically Quantized Solitons of the One-Dimensional Easy-Axis Néel State. *Phys. Rev. Lett.* **50**, 1153 (1983). <https://doi.org/10.1103/PhysRevLett.50.1153>

- 1103/PhysRevLett.50.1153
- 3 Affleck, I., Kennedy, T., Lieb, E. H., & Tasaki, H. Rigorous results on valence-bond ground states in antiferromagnets. *Phys. Rev. Lett.* **59**, 799 (1987). <https://doi.org/10.1103/PhysRevLett.59.799>
  - 4 Johnston, D. C. The puzzle of high temperature superconductivity in layered iron pnictides and chalcogenides. *Adv. Phys.* **59**, 803 (2010). <https://doi.org/10.1080/00018732.2010.513480>.
  - 5 Fernandes, R. M. & Chubukov, A. V. Low-energy microscopic models for iron-based superconductors: a review. *Rep. Prog. Phys.* **80**, 014503 (2017). <http://stacks.iop.org/0034-4885/80/i=1/a=014503>.
  - 6 Dai, P., Hu, J. & Dagotto, E. Magnetism and its microscopic origin in iron-based high-temperature superconductors. *Nature Physics* **85**, 709 (2012). <http://dx.doi.org/10.1038/nphys2438>.
  - 7 Dagotto, E. Colloquium: The unexpected properties of alkali metal iron selenide superconductors. *Rev. Mod. Phys.* **85**, 849 (2013). <https://link.aps.org/doi/10.1103/RevModPhys.85.849>.
  - 8 Tun, Z. *et al.* Haldane-gap modes in the S=1 antiferromagnetic chain compound CsNiCl<sub>3</sub>. *Phys. Rev. B* **42**, 4677 (1990). <https://doi.org/10.1103/PhysRevB.42.4677>
  - 9 Mutka, H. *et al.* Dynamic structure factor  $[S(Q,\omega)]$  of the S=1 quasi-one-dimensional Heisenberg antiferromagnet: Neutron-scattering study on AgVP<sub>2</sub>S<sub>6</sub>. *Phys. Rev. Lett.* **67**, 497 (1991). <https://doi.org/10.1103/PhysRevLett.67.497>
  - 10 Ma, S.-L. *et al.* Dominance of long-lived excitations in the antiferromagnetic spin-1 chain NENP. *Phys. Rev. Lett.* **69**, 3571 (1992). <https://doi.org/10.1103/PhysRevLett.69.3571>
  - 11 Di Tusa, J.F. *et al.* Magnetic and Charge Dynamics in a Doped One-Dimensional Transition Metal Oxide. *Phys. Rev. Lett.* **73**, 1857 (1994). <https://doi.org/10.1103/PhysRevLett.73.1857>
  - 12 Uchiyama, Y. *et al.* Spin-Vacancy-Induced Long-Range Order in a New Haldane-Gap Antiferromagnet. *Phys. Rev. Lett.* **83**, 632 (1999). <https://doi.org/10.1103/PhysRevLett.83.632>
  - 13 Golinelli, O., Jolicoeur, Th., & Lacaze, R. Dispersion of magnetic excitations in a spin-1 chain with easy-plane anisotropy. *Phys. Rev. B* **46**, 10854 (1992). <https://doi.org/10.1103/PhysRevB.46.10854>
  - 14 White, S. R. & Huse, D. A. Numerical renormalization-group study of low-lying eigenstates of the antiferromagnetic S=1 Heisenberg chain. *Phys. Rev. B* **48**, 3844 (1993). <https://doi.org/10.1103/PhysRevB.48.3844>
  - 15 For a recent review of Haldane chains see Jolicoeur Th. & Golinelli O., Physics of integer-spin antiferromagnetic chains: Haldane gaps and edge states. *Comptes Rendus Chimie* **22**, 445 (2019). <https://doi.org/10.1016/j.crci.2019.05.005>
  - 16 Dagotto, E. Correlated electrons in high-temperature superconductors. *Rev. Mod. Phys.* **66**, 763 (1994), and references therein. <https://doi.org/10.1103/RevModPhys.66.763>
  - 17 Scalapino, D. J. A common thread: The pairing interaction for unconventional superconductors. *Rev. Mod. Phys.* **84**, 1383 (2012), and references therein. <https://doi.org/10.1103/RevModPhys.84.1383>
  - 18 Dagotto, E., Riera, J. A. & Scalapino, D. J. Superconductivity in ladders and coupled planes. *Phys. Rev. B* **45**, 5744(R) (1992). <https://doi.org/10.1103/PhysRevB.45.5744>
  - 19 Dagotto, E., & Rice, T. M. Surprises on the Way from One- to Two-Dimensional Quantum Magnets: The Ladder Materials. *Science* **271**, 618 (1996). <https://doi.org/10.1126/science.271.5249.618>
  - 20 Dagotto, E. Experiments on ladders reveal a complex interplay between a spin-gapped normal state and superconductivity. *Rep. Prog. Phys.* **62**, 1525 (1999). <https://doi.org/10.1088/0034-4885/62/11/202>
  - 21 Uehara, M., Nagata, T., Akimitsu, J., Takahashi, H., Mori, N., & Kinoshita, K. Superconductivity in the Ladder Material Sr<sub>14-x</sub>Ca<sub>x</sub>Cu<sub>24</sub>O<sub>41.84</sub>. *J. Phys. Soc. Jpn.* **65**, 2764 (1996). <https://doi.org/10.1143/JPSJ.65.2764>
  - 22 Piskunov, Y., Jérôme, D., Auban-Senzier, P., Wzietek, P., & Yakubovsky, A. Hole redistribution in Sr<sub>14-x</sub>Ca<sub>x</sub>Cu<sub>24</sub>O<sub>41</sub> ( $x=0,12$ ) spin ladder compounds: <sup>63</sup>Cu and <sup>17</sup>O NMR studies under pressure. *Phys. Rev. B* **72**, 064512 (2005). <https://doi.org/10.1103/PhysRevB.72.064512>
  - 23 Takahashi, H. *et al.* Pressure-induced superconductivity in the iron-based ladder material BaFe<sub>2</sub>S<sub>3</sub>. *Nature Materials* **14**, 1008 (2015). <http://dx.doi.org/10.1038/nmat4351>.
  - 24 Yamauchi, T., Hirata, Y., Ueda, Y. & Ohgushi, K. Pressure-induced Mott transition followed by a 24-K superconducting phase in BaFe<sub>2</sub>S<sub>3</sub>. *Phys. Rev. Lett.* **115**, 246402 (2015). <https://link.aps.org/doi/10.1103/PhysRevLett.115.246402>.
  - 25 Zhang, Y., Lin, L.-F., Zhang, J.-J., Dagotto, E., & Dong, S. Pressure-driven phase transition from antiferromagnetic semiconductor to nonmagnetic metal in the two-leg ladders AFe<sub>2</sub>X<sub>3</sub> (A=Ba,K; X=S,Se). *Phys. Rev. B* **95**, 115154 (2017). <https://doi.org/10.1103/PhysRevB.95.115154>
  - 26 Ying, J., Lei, H., Petrovic, C., Xiao, Y. & Struzhkin, V. V. Interplay of magnetism and superconductivity in the compressed Fe-ladder compound BaFe<sub>2</sub>Se<sub>3</sub>. *Phys. Rev. B* **95**, 241109 (2017). <https://link.aps.org/doi/10.1103/PhysRevB.95.241109>.
  - 27 Zhang, Y., Lin, L.-F., Zhang, J.-J., Dagotto, E. & Dong, S. Sequential structural and antiferromagnetic transitions in BaFe<sub>2</sub>Se<sub>3</sub> under pressure. *Phys. Rev. B* **97**, 045119 (2018). <https://link.aps.org/doi/10.1103/PhysRevB.97.045119>.
  - 28 Caron, J. M., Neilson, J. R., Miller, D. C., Llobet, A. & McQueen, T. M. Iron displacements and magnetoelastic coupling in the antiferromagnetic spin-ladder compound BaFe<sub>2</sub>Se<sub>3</sub>. *Phys. Rev. B* **84**, 180409 (2011). <https://link.aps.org/doi/10.1103/PhysRevB.84.180409>.
  - 29 Lei, H., Ryu, H., Frenkel, A. I. & Petrovic, C. Anisotropy in BaFe<sub>2</sub>Se<sub>3</sub> single crystals with double chains of FeSe tetrahedra. *Phys. Rev. B* **84**, 214511 (2011). <https://link.aps.org/doi/10.1103/PhysRevB.84.214511>.
  - 30 Nambu, Y. *et al.* Block magnetism coupled with local distortion in the iron-based spin-ladder compound BaFe<sub>2</sub>Se<sub>3</sub>. *Phys. Rev. B* **85**, 064413 (2012). <https://link.aps.org/doi/10.1103/PhysRevB.85.064413>.
  - 31 Caron, J. M. *et al.* Orbital-selective magnetism in the spin-ladder iron selenides Ba<sub>1-x</sub>K<sub>x</sub>Fe<sub>2</sub>Se<sub>3</sub>. *Phys. Rev. B* **85**, 180405 (2012). <https://link.aps.org/doi/10.1103/PhysRevB.85.180405>.
  - 32 Du, F., Ohgushi, K., Nambu, Y., Kawakami, T., Avdeev, M., Hirata, Y., Watanabe, Y., Sato, T. J. & Ueda, Y. Stripelike magnetism in a mixed-valence insulating state of the Fe-based ladder compound CsFe<sub>2</sub>Se<sub>3</sub>. *Phys. Rev. B*

- 85, 214436 (2012). <https://doi.org/10.1103/PhysRevB.85.214436>
- <sup>33</sup> Luo, Q. *et al.* Magnetic states of the two-leg-ladder alkali metal iron selenides  $\text{AFe}_2\text{Se}_3$ . *Phys. Rev. B* **87**, 024404 (2013). <https://link.aps.org/doi/10.1103/PhysRevB.87.024404>.
- <sup>34</sup> Dong, S., Liu, J.-M., & Dagotto E.,  $\text{BaFe}_2\text{Se}_3$ : A High  $T_C$  Magnetic Multiferroic with Large Ferrielectric Polarization. *Phys. Rev. Lett.* **113**, 187204 (2014). <https://doi.org/10.1103/PhysRevLett.113.187204>
- <sup>35</sup> Arita, R., Ikeda, H., Sakai, S., & Suzuki, M.-T. *Ab initio* downfolding study of the iron-based ladder superconductor  $\text{BaFe}_2\text{S}_3$ . *Phys. Rev. B* **92**, 054515 (2015). <https://doi.org/10.1103/PhysRevB.92.054515>
- <sup>36</sup> Suzuki, M.-T., Arita, R., & Ikeda H. First-principles study of magnetic properties in Fe-ladder compound  $\text{BaFe}_2\text{S}_3$ . *Phys. Rev. B* **92**, 085116 (2015). <https://doi.org/10.1103/PhysRevB.92.085116>
- <sup>37</sup> Mourigal, M. *et al.* Block magnetic excitations in the orbitally selective Mott insulator  $\text{BaFe}_2\text{Se}_3$ . *Phys. Rev. Lett.* **115**, 047401 (2015). <https://link.aps.org/doi/10.1103/PhysRevLett.115.047401>.
- <sup>38</sup> Patel, N. D. *et al.* Magnetic properties and pairing tendencies of the iron-based superconducting ladder  $\text{BaFe}_2\text{S}_3$ : Combined *ab initio* and density matrix renormalization group study. *Phys. Rev. B* **94**, 075119 (2016). <https://link.aps.org/doi/10.1103/PhysRevB.94.075119>.
- <sup>39</sup> Chi, S., Uwatoko, Y., Cao, H., Hirata, Y., Hashizume, K., Aoyama, T., & Ohgushi, K. Magnetic Precursor of the Pressure-Induced Superconductivity in Fe-Ladder Compounds. *Phys. Rev. Lett.* **117**, 047003 (2016). <https://doi.org/10.1103/PhysRevLett.117.047003>
- <sup>40</sup> Wang, M. *et al.* Spin waves and magnetic exchange interactions in the spin-ladder compound  $\text{RbFe}_2\text{Se}_3$ . *Phys. Rev. B* **94**, 041111(R) (2016). <https://doi.org/10.1103/PhysRevB.94.041111>
- <sup>41</sup> Wang, M. *et al.* Strong ferromagnetic exchange interaction under ambient pressure in  $\text{BaFe}_2\text{S}_3$ . *Phys. Rev. B* **95**, 060502(R) (2017). <https://doi.org/10.1103/PhysRevB.95.060502>
- <sup>42</sup> Takubo, K. *et al.* Orbital order and fluctuations in the two-leg ladder materials  $\text{BaFe}_2\text{X}_3$  ( $\text{X}=\text{S}$  and  $\text{Se}$ ) and  $\text{CsFe}_2\text{Se}_3$ . *Phys. Rev. B* **96**, 115157 (2017). <https://doi.org/10.1103/PhysRevB.96.115157>
- <sup>43</sup> Seidov, Z. *et al.* Magnetic susceptibility and ESR study of the covalent-chain antiferromagnets  $\text{TlFeS}_2$  and  $\text{TlFeSe}_2$ . *Phys. Rev. B* **65**, 014433 (2001). <https://doi.org/10.1103/PhysRevB.65.014433>.
- <sup>44</sup> Welz, D. & M. Nishi, M. Spin, exchange, and anisotropy in the covalent-chain antiferromagnet  $\text{TlFeS}_2$ . *Phys. Rev. B* **45**, 9806 (1992). <https://doi.org/10.1103/PhysRevB.45.9806>
- <sup>45</sup> Luo, Q. *et al.* Magnetic states of the five-orbital Hubbard model for one-dimensional iron-based superconductors. *Phys. Rev. B* **90**, 035128 (2014), and references therein. <https://doi.org/10.1103/PhysRevB.90.035128>
- <sup>46</sup> White, S. R. Density matrix formulation for quantum renormalization groups. *Phys. Rev. Lett.* **69**, 2863 (1992). <https://link.aps.org/doi/10.1103/PhysRevLett.69.2863>.
- <sup>47</sup> Schollwöck, U. The density-matrix renormalization group in the age of matrix product states. *Annals of Physics* **326**, 96 (2011). <https://doi.org/10.1016/j.aop.2010.09.012>.
- <sup>48</sup> White, S. R. Density matrix renormalization group algorithms with a single center site. *Phys. Rev. B* **72**, 180403 (2005). <https://link.aps.org/doi/10.1103/PhysRevB.72.180403>.
- <sup>49</sup> Alvarez, G. The density matrix renormalization group for strongly correlated electron systems: A generic implementation. *Computer Physics Communications* **180**, 1572 (2009). <https://doi.org/10.1016/j.cpc.2009.02.016>.
- <sup>50</sup> Riera, J., Hallberg, K., & Dagotto, E. Phase Diagram of Electronic Models for Transition Metal Oxides in One Dimension. *Phys. Rev. Lett.* **79**, 713 (1997). <https://doi.org/10.1103/PhysRevLett.79.713>
- <sup>51</sup> Shirakawa, T., Nishimoto, S. & Ohta, Y. Superconductivity in a model of two Hubbard chains coupled with ferromagnetic exchange interaction. *Phys. Rev. B* **77**, 224510 (2008). <https://doi.org/10.1103/PhysRevB.77.224510>
- <sup>52</sup> Xavier, J. C., Alvarez, G., Moreo, A. & Dagotto, E. Coexistence of pairing tendencies and ferromagnetism in a doped two-orbital Hubbard model on two-leg ladders. *Phys. Rev. B* **81**, 085106 (2010). <https://doi.org/10.1103/PhysRevB.81.085106>
- <sup>53</sup> Patel, N. D., Nocera, A., Alvarez, G., Moreo, A. & Dagotto, E. Pairing tendencies in a two-orbital Hubbard model in one dimension. *Phys. Rev. B* **96**, 024520 (2017). <https://link.aps.org/doi/10.1103/PhysRevB.96.024520>.
- <sup>54</sup> Jiang, H.-C., Li, Z.-X., Seidel, A., & Lee, D.-H. Symmetry protected topological Luttinger liquids and the phase transition between them. *Science Bulletin* **63**, 753 (2018) <https://doi.org/10.1016/j.scib.2018.05.010>
- <sup>55</sup> Anderson, P. W. The Resonating Valence Bond State in  $\text{La}_2\text{CuO}_4$  and Superconductivity. *Science* **235**, 1196 (1987). <https://doi.org/10.1126/science.235.4793.1196>
- <sup>56</sup> Anderson, P. W. *et al.* Resonating valence-bond theory of phase transitions and superconductivity in  $\text{La}_2\text{CuO}_4$ -based compounds. *Phys. Rev. Lett.* **58**, 2790 (1987). <https://doi.org/10.1103/PhysRevLett.58.2790>
- <sup>57</sup> Mackenzie, A. P. & Maeno, Y. The superconductivity of  $\text{Sr}_2\text{RuO}_4$  and the physics of spin-triplet pairing. *Rev. Mod. Phys.* **75**, 657 (2003). <https://doi.org/10.1103/RevModPhys.75.657>
- <sup>58</sup> Strand, J. D. *et al.* The Transition Between Real and Complex Superconducting Order Parameter Phases in  $\text{UPt}_3$ . *Science* **328**, 1368 (2010). <https://doi.org/10.1126/science.1187943>
- <sup>59</sup> Ran, S. *et al.* Nearly ferromagnetic spin-triplet superconductivity. *Science* **365**, 684 (2019). <https://doi.org/10.1126/science.aav8645>
- <sup>60</sup> Herbrych, J. *et al.* Spin dynamics of the block orbital-selective Mott phase. *Nat. Commun.* **9**, 3736 (2018). <https://doi.org/10.1038/s41467-018-06181-6>
- <sup>61</sup> Patel, N. D. *et al.* Fingerprints of an orbital-selective Mott phase in the block magnetic state of  $\text{BaFe}_2\text{Se}_3$  ladders. *Communications Physics* **2**, Article number: 64 (2019). <https://doi.org/10.1038/s42005-019-0155-3>
- <sup>62</sup> Herbrych, J., Heverhagen, J., Patel, N. D., Alvarez, G., Daghofer, M., Moreo, A. & Dagotto, E. Novel Magnetic Block States in Low-Dimensional Iron-Based Superconductors. *Phys. Rev. Lett.* **123**, 027203 (2019). <https://doi.org/10.1103/PhysRevLett.123.027203>
- <sup>63</sup> Yin, Z. P., Haule, K. & Kotliar, G. Kinetic frustration and the nature of the magnetic and paramagnetic states in iron pnictides and iron chalcogenides. *Nat. Mater.* **10**,

- 932 (2011). <https://doi.org/10.1038/nmat3120>
- <sup>64</sup> Luo, Q. *et al.* Neutron and ARPES constraints on the couplings of the multi-orbital Hubbard model for the iron pnictides. *Phys. Rev. B* **82**, 104508 (2010). <https://doi.org/10.1103/PhysRevB.82.104508>
- <sup>65</sup> Li, H. & Haldane, F. D. M. Entanglement spectrum as a generalization of entanglement entropy: Identification of topological order in non-abelian fractional quantum hall effect states. *Phys. Rev. Lett.* **101**, 010504 (2008). <https://doi.org/10.1103/PhysRevLett.101.010504>
- <sup>66</sup> Miyakoshi, S., Nishimoto, S., & Ohta, Y. Entanglement properties of the Haldane phases: A finite system-size approach. *Phys. Rev. B* **94**, 235155 (2016), and references therein. <https://doi.org/10.1103/PhysRevB.94.235155>
- <sup>67</sup> Pollmann, F., Turner, A. M., Berg, E., & Oshikawa, M. Entanglement spectrum of a topological phase in one dimension. *Phys. Rev. B* **81**, 064439 (2010). <https://doi.org/10.1103/PhysRevB.81.064439>
- <sup>68</sup> Barthel, T., Chung, M.-C., & Schollwöck, U. Entanglement scaling in critical two-dimensional fermionic and bosonic systems. *Phys. Rev. A* **74**, 022329 (2006). <https://doi.org/10.1103/PhysRevA.74.022329>
- <sup>69</sup> Eisert, J., Cramer, M. & Plenio, M. B. Colloquium: Area laws for the entanglement entropy. *Rev. Mod. Phys.* **82**, 277 (2010), and references therein. <https://doi.org/10.1103/RevModPhys.82.277>
- <sup>70</sup> Li, W., Weichselbaum, A. & von Delft, J. Identifying symmetry-protected topological order by entanglement entropy. *Phys. Rev. B* **88**, 245121 (2013). <https://doi.org/10.1103/PhysRevB.88.245121>
- <sup>71</sup> Martins, G. B. *et al.* Doped Stripes in Models for the Cuprates Emerging from the One-Hole Properties of the Insulator. *Phys. Rev. Lett.* **84**, 5844 (2000). <https://doi.org/10.1103/PhysRevLett.84.5844>
- <sup>72</sup> Martins, G. B. *et al.* Indications of spin-charge separation at short distance and stripe formation in the extended t-J model on ladders and planes. *Phys. Rev. B* **63**, 014414 (2000). <https://doi.org/10.1103/PhysRevB.63.014414>
- <sup>73</sup> Ogata, M. & Shiba, H. Bethe-ansatz wave function, momentum distribution, and spin correlation in the one-dimensional strongly correlated Hubbard model *Phys. Rev. B* **41**, 2326 (1990). <https://doi.org/10.1103/PhysRevB.41.2326>
- <sup>74</sup> White, S. R. & Scalapino, D. J. Hole and pair structures in the t-J model *Phys. Rev. B* **55**, 6504 (1997). <https://doi.org/10.1103/PhysRevB.55.6504>